A Study of the Reaction of N^+ with O_2: Experimental Quantification of $NO^+(a\ ^3\Sigma^+)$ Production (298−500 K) and Computational Study of the Overall Reaction Pathways†

Anthony J. Midey‡ and A. A. Viggiano*

Air Force Research Laboratory, Space Vehicles Directorate, 29 Randolph Rd., Hanscom Air Force Base, Massachusetts 01731-3010

Peng Zhang, Stephan Irle, and Keiji Morokuma*

Cherry L. Emerson Center for Scientific Computation and Department of Chemistry, Emory University, Atlanta, Georgia 30322

Received: August 5, 2005; In Final Form: September 12, 2005

The product branching ratios for $NO^+(X\ ^1\Sigma^+)$ and $NO^+(a\ ^3\Sigma^+)$ produced from the reaction of N^+ with O_2 have been measured at 298 and 500 K in a selected ion flow tube. Approximately 0.5% of the total products are in $NO^+(a)$ at both temperatures, despite the fact that the reaction to form $NO^+(a)$ is 0.3 eV exothermic. High-level ab initio calculations of the potential energy surfaces for the $N^+ + O_2$ reaction show that the reaction from $N^+(^3P) + O_2(^3\Sigma_g)$ reactants starts with an efficient early stage charge transfer to the $N(^2D) + O_2^+(X\ ^2\Pi)$ channel, which gives rise to the $O_2^+(X\ ^2\Pi)$ product and, at the same time, serves as the starting point for all of the reaction channels leading to NO^+ and O^+ products. Pathways to produce $NO^+(a\ ^3\Sigma^+)$ are found to be less favorable than pathways leading to the major product $NO^+(X\ ^1\Sigma^+)$. Production of $N(^2D)$ has implications for the concentration of NO in the mesosphere.

Introduction

N^+ ions are readily formed in the earth's ionosphere and are one of the major species found at altitudes of 200−400 km.[1] In addition, the reaction of N^+ with O_2 is the primary sink for this ion in the atmosphere.[2,3] Consequently, it has been extensively studied with a variety of techniques,[4−18] particularly to elucidate the energy dependence of the kinetics[4,6,13,19] and the product distributions.[5,10,17,19]

The rate constants for the N^+ reaction with O_2 are well established as a function of temperature[4,6,19] and kinetic energy.[10,13,14] The rate constants measured in a drift tube are independent of the center of mass kinetic energy, having a value of $\sim 5.5 \times 10^{-10}$ cm^3 s^{-1}.[10,13,14] Recent flow tube measurements as a function of temperature show that the rate constants agree with drift tube values from 200 to 1000 K and then increase slightly up to 1400 K, where the rate constant is ca. 15% higher than drift tube data at the same kinetic energy. While this difference is within the experimental error, it is also consistent with an enhancement of the rate constant for vibrationally excited O_2 ($v > 0$) to the collision rate, almost double the $v = 0$ rate constant.[19]

The temperature[19] and kinetic energy dependences[5,10] of the branching ratios have been examined as well. Several products ions have been observed as outlined in eqs 1a−e. The branching ratios are well established to be ca. 50% O_2^+, ca. 40% NO^+ (total), and 10% O^+ near room temperature.[10,15,17,19] The O_2^+ product channel increases at the expense of the NO^+ channel at collision energies above ~0.15 eV, accounting for >70% of the products above 0.6 eV.[10,17]

$$N^+(^3P) + O_2(X\ ^3\Sigma_g) \rightarrow O^+(^4S) + NO(X\ ^2\Pi) + 2.3\ eV \quad (1a)$$

$$\rightarrow O_2^+(X\ ^2\Pi_g) + N(^4S) + 2.5\ eV \quad (1b)$$

$$\rightarrow NO^+(X\ ^1\Sigma^+) + O(^3P) + 6.7\ eV \quad (1c)$$

$$\rightarrow NO^+(a\ ^3\Sigma^+) + O(^3P) + 0.3\ eV \quad (1d)$$

$$\rightarrow O_2^+(X\ ^2\Pi_g) + N(^2D) + 0.04\ eV \quad (1e)$$

Formation of the NO^+ product in its first excited electronic state, i.e., $NO^+(a\ ^3\Sigma^+)$, is 0.3 eV exothermic. Albritton et al.[9] have previously used a selected ion flow tube (SIFT) at 298 K to investigate the branching into the two accessible electronic states given in eqs 1c,d. They have exploited the difference in reactivity between the $NO^+(a)$ and $NO^+(X)$ states[20−22] to estimate that the $NO^+(a)$ state contributes to ≤5% of the NO^+ products observed in reaction 1 or ≤2% of the total products.[9]

While very little $NO^+(a\ ^3\Sigma^+)$ has been observed at room temperature despite its exothermicity,[9] it is possible that the production of this excited state will increase at higher temperatures since more energy is available for reaction. To address this issue, the difference in reactivity of the lowest two NO^+ electronic states has again been utilized to probe the amount of $NO^+(a\ ^3\Sigma^+)$ generated at 298 and 500 K in a SIFT. Only a small fraction of the NO^+ ions are formed in the a state at 298 K, in agreement with the previous measurements,[9] with no measurable increase at 500 K. Ab initio calculations of the overall potential energy surfaces for the N^+ reaction with O_2 are consistent with the experimental results. The calculations show that reaction 1d proceeds through a very complicated

† Part of the special issue "Juergen Troe Festschrift".

* Corresponding authors.

‡ Under contract to Institute for Scientific Research, Boston College, Chestnut Hill, MA.

10.1021/jp054376g CCC: $33.50
Published on Web 10/21/2005

pathway involving numerous excited electronic states without a facile path to the $NO^+(a\ ^3\Sigma^+)$ state. The calculations also show that the N atoms produced in reaction 1 are more favorably produced in the excited $N(^2D)$ state (reaction 1e), which has implications for ionospheric NO chemistry.

Methods

(a) SIFT Experiments. The selected ion flow tube (SIFT) has been described at length elsewhere[23] so only the details relevant to the current measurements will be discussed. Electron impact on N_2 in an effusive ion source creates N^+ ions that are selected by a quadrupole mass filter and injected into a fast flow of helium (99.997%, AGA Gas) through a Venturi inlet. Argon gas (99.999%, Matheson) is introduced into the flow tube 30 cm upstream of the reactant inlet to quench any N^+ metastables produced in the source and subsequently to scavenge the $NO^+(a\ ^3\Sigma^+)$ generated by the reaction of N^+ with O_2 (99.999%, Mass. Oxygen) in the reaction region. Previous flow tube measurements show that ≥85% of the reaction products of $NO^+(a\ ^3\Sigma^+)$ with Ar forms Ar^+, while the remainder is quenched to $NO^+(X)$.[21] The maximum O_2 flow is adjusted to optimize the depletion of N^+,[19] while minimizing the reaction of Ar^+ scavenger ions with O_2, which is over 10 times slower than the N^+ reaction with O_2.[24] Typically, a maximum flow of 1 sccm O_2 reactant gas and a fixed flow of 150 sccm Ar (∼1% of the buffer) scavenger gas have been used in the current experiments. At the end of the reaction zone, the reactant and product ions are sampled through a blunt nose cone aperture, analyzed with a quadrupole mass filter, and detected.

The amount of $NO^+(a\ ^3\Sigma^+)$ product created in reaction 1 is determined as follows. Kinetics data as a function of O_2 concentration at a fixed Ar concentration are taken at mass resolution settings low enough to minimize mass discrimination but high enough to resolve NO^+ at *m*/*z* 30 and O_2^+ at *m*/*z* 32. The ratio of NO^+ to Ar^+ is obtained from the branching ratios extrapolated to zero O_2 flow rate, a method that accounts for any secondary chemistry that may occur at larger O_2 flows. The small Ar^+ signal at zero O_2 flow resulting from quenching of energetic species is subtracted from the Ar^+ total counts, and the branching ratios are renormalized. This Ar^+ background contribution is <4% of the reactant ion signal and is unaffected by opening or closing the valve after the O_2 flow controller, i.e., does not result from O_2 leaking into the flow tube. The Ar^+ signal is also corrected for the fact that when $NO^+(a\ ^3\Sigma^+)$ reacts with Ar, only 85% of the reactivity is due to charge transfer.[21]

(b) Computational Details. Stationary points on the potential energy surfaces for reaction 1 were optimized using numerical gradient techniques at the state-specific complete active space CASPT2 level of theory[25] using Dunning's correlation consistent polarized valence triple-ζ basis sets, cc-pVTZ.[26] In the internally contracted second-order multireference perturbation (CASPT2) calculations[25] the 1*s* orbitals of the N and O atoms were kept doubly occupied in all configurations and the remaining 16 electrons were correlated, denoted as CASPT2(16e/12o). Here we adopted Anderson's g_4 Fock operator as the zero-order Hamiltonian for the CASPT2 calculations, on top of a reference space at the state-specific CASSCF(16e/12o)/ cc-pVTZ level, for which the CASPT2 calculations are size-extensive for cases where a molecule dissociates to high-spin open-shell atoms. Finally, single point energy calculations at the internally contracted multireference configuration interaction level with single and double excitations[27] (MRCISD) plus Davidson correction[28,29] (Q) were performed with Dunning's augmented correlation consistent polarized valence quadruple-ζ basis set, aug-cc-pVQZ, using the molecular orbital and reference configurations from the predetermined state-specific CASSCF(16e/12o)/aug-cc-pVQZ wave function. Similar to CASPT2, only the 1*s* orbitals of N and O atoms were kept doubly occupied in all configurations and the remaining 16 electrons were correlated, denoted as MRCISD(Q)(16e/12o). The Molpro 2002.6 quantum chemistry package was used to perform all these calculations.

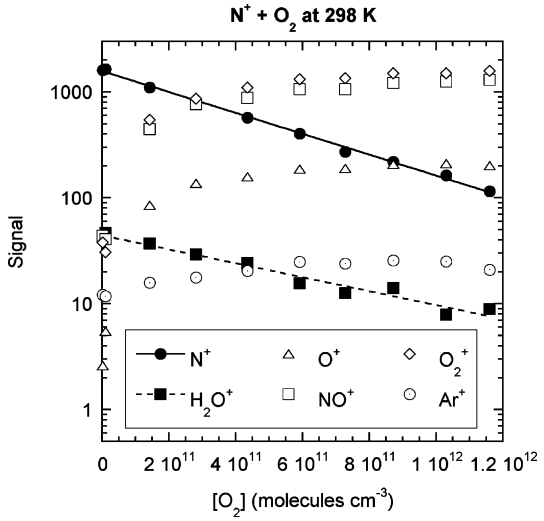

Figure 1. Typical kinetics data for the reaction of N^+ with O_2 giving O^+, O_2^+, and NO^+ as products. The H_2O^+ arises from a small water impurity and can be corrected in the branching ratios. The Ar^+ is from the secondary reaction of NO^+* with Ar scavenger gas. (See text for details.)

Results and Discussion

(a) Experimental Results. Figure 1 shows typical kinetics data from the SIFT at 298 K using Ar as a scavenger. A ≤ 4% H_2O^+ signal is observed from trace amounts of an H_2O impurity. H_2O^+ reacts with O_2 to give O_2^+,[30] but it does not react with Ar so a correction can be made to the overall branching ratios. However, making this correction will not affect the ratio of NO^+ to Ar^+. The overall branching fractions at 298 K are 0.50 for O_2^+, 0.42 NO^+ (total) and 0.08 O^+ at 298 K in good agreement with the previous measurements.[10,17,19] However, only ∼1% of NO^+ product ions are generated in the 1st electronic excited state ($a\ ^3\Sigma^+$), compared to the limit of ≤ 5% determined by Albritton et al.[9] Interestingly, the amount of NO^+ ($a\ ^3\Sigma^+$) at 500 K is also ∼1% of the NO^+ products. Since NO^+ is only 42% of the total products, the reaction produces about 0.4−0.5% NO^+ ($a\ ^3\Sigma^+$) overall.

To test for possible uncertainties, several flow tube conditions have been varied at 500 K including the electron energy, the ion injection energy, source lens voltages, flow tube pressure, and the quadrupole resolution settings. None of these variations substantially changes the ratio of $NO^+(a\ ^3\Sigma^+)$ to $NO^+(X\ ^1\Sigma^+)$ detected. Thus, increasing the temperature to 500 K does not increase the amount of electronically excited NO^+ ion created in the reaction of N^+ with O_2, indicating that increasing the available translational and rotational energy does not drive this channel. Little vibrational excitation (∼1%) of the O_2 occurs at 500 K.

We have not remeasured the overall branching ratios at 500 K. However, the branching ratios have been shown to be essentially independent of energy and temperature in the range covered by these experiments[10,17,19] and the experimental conditions are similar to our recent SIFT experiments.[19] An

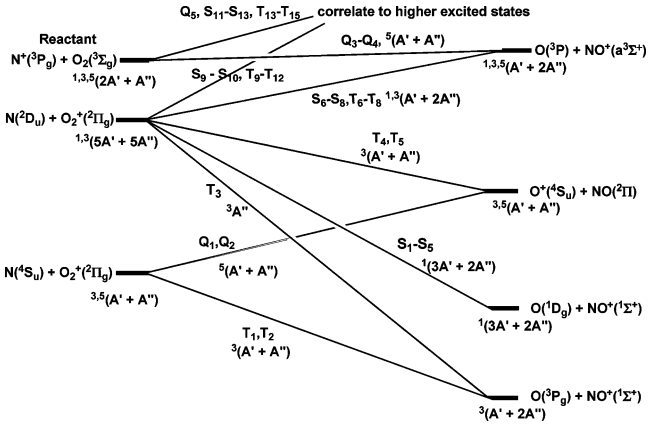

Figure 2. Adiabatic electronic state correlation relationships between low-lying states of the $[N + O_2]^+$ limit and those of the $[O + NO]^+$ limit in C_s symmetry. (See text for details.)

additional consideration is that the NO^+ ($a\ ^3\Sigma^+$) can undergo secondary reactions with O_2 in competition with quenching by Ar.[20,22] NO^+($a\ ^3\Sigma^+$) reacts with O_2 to quench the excitation, producing NO^+(X).[20,22] The total rate constant for the O_2 reaction with NO^+ ($a\ ^3\Sigma^+$) is an order of magnitude higher than that for the Ar reaction.[20,22] Consequently, the Ar flow rates have been kept at least 150 times higher than the maximum O_2 flow, so that the NO^+ ($a\ ^3\Sigma^+$) product ions react at least 15 times more often with Ar than with O_2. The O^+ and O_2^+ products are presumably generated in their ground electronic states, which do not react with Ar. In addition, the O^+ charge-transfer reaction with O_2 is quite slow, $<2 \times 10^{-11}$ $cm^3\ s^{-1}$, and should not interfere either.[4,13,31] NO^+(X) is similarly unreactive with both Ar and O_2.[30]

These potential interferences have also been addressed in the previous measurements of Albritton et al. of the NO^+($a\ ^3\Sigma^+$) state distribution.[9] At very small fractions of NO^+($a\ ^3\Sigma^+$), the amount of NO^+* found using a simple first order model accounting for only the initial N^+ reaction and the scavenger reaction gives essentially the same result as a complete model accounting for all secondary reactions.[9] We have used the first-order approach, which is acceptable given the very small value and the other typical uncertainties in the current experiments.

(b) Computational Results and Reaction Mechanism. The overall reaction mechanism giving the various product channels of reaction 1 determined by ab initio calculations is discussed individually for each product channel in this section. The notation S_n, T_n, and Q_n will be used to represent the *n*th singlet, triplet, and quintet potential surfaces/pathways, respectively.

(1) $N(^2D) + O_2^+(X\ ^2\Pi_g)$ Charge-Transfer Product. Figure 2 shows the adiabatic electronic state correlation relationships between low-lying states of the $[N + O_2]^+$ limit and those of the $[O + NO]^+$ limit in the C_s symmetry. The reactant $N^+(^3P) + O_2(X\ ^3\Sigma_g)$ states, which are singlet S_{11} to S_{13}, triplet T_{13} to T_{15} and quintet Q_3 to Q_5, adiabatically correlate mostly to highly excited states but not directly to any of the product states observed in the experiments, except for $O(^3P) + NO^+(a\ ^3\Sigma^+)$ through Q_3 and Q_4. The potential energy curve of the $N^+(^3P) + O_2(X\ ^3\Sigma_g)$ ($S_{11}-S_{13}$, $T_{13}-T_{15}$, Q_3-Q_5) manifold and that of the energetically very close $N(^2D) + O_2^+(X\ ^2\Pi)$ (S_6-S_{10}, T_6-T_{12}) manifold calculated at varying O−O bond distances with infinite N···O_2 separation are shown in Figure 3. The two potential curves have a crossing at around $R_{OO} = 1.20$ Å (2.25 bohr). This means that charge transfer from N^+ in $N^+(^3P) + O_2(X\ ^3\Sigma_g)$ to O_2 to give $N(^2D) + O_2^+(X\ ^2\Pi)$ can take place at this O−O distance. Since the energy of crossing is almost the same as the $O_2(X\ ^3\Sigma_g)$ zero-point energy (~0.1 eV), this crossing point will be sampled every time the O_2 molecule vibrates. At infinite separation, however, the nonadiabatic coupling element between these two manifolds is zero. As the N^+ ion approaches, the degeneracy of these states will be lifted and a nonvanishing coupling element will arise between states with the same spin symmetry. As a result, the charge transfer process will take place. Determining the location of the seams of crossing for tens of different state combinations is costly, and we have not performed such calculations. However, our previous experience suggests that the energy of crossing at finite separation is not much different from that at infinite separation.[32,33] In the present case, the energy of "the transition state" for charge transfer is expected to be extremely close to the reactant energy at the early stage of the $[N-O_2]^+$ entrance channel. Therefore, the charge transfer process is expected to be a highly efficient process, which serves as the starting point for the rest of the chemistry after dissociation occurs. Assuming all the observed channels start from this channel, the experiment indicates the efficiency of this charge transfer process is approximately 60%, i.e., the overall experimental reaction efficiency. Simple dissociation of the collision complex after charge transfer then leads to the $N(^2D) + O_2^+(X\ ^2\Pi_g)$ product, which is the major product of the present reaction.

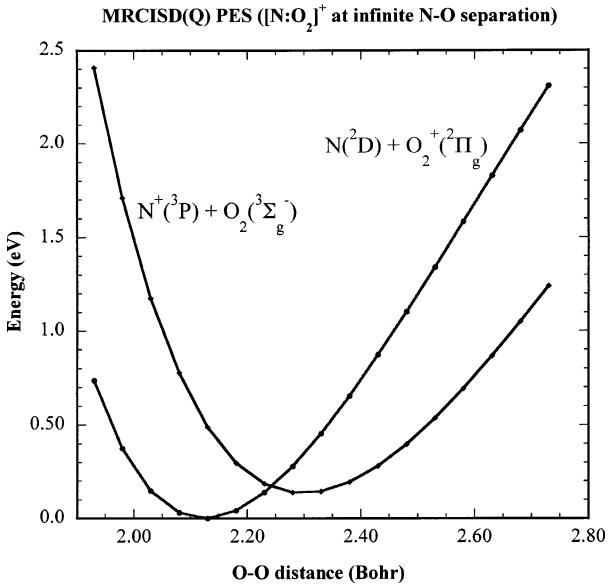

Figure 3. Potential energy curve of the $N^+(^3P) + O_2(X\ ^3\Sigma_g)$ ($S_{11}-S_{13}$, $T_{13}-T_{15}$, Q_3-Q_5) manifold and that of the $N(^2D) + O_2^+(X\ ^2\Pi)$ (S_6-S_{10}, T_6-T_{12}) manifold calculated at varying O−O bond distance at the infinite N···O_2 separation at the MRCISD(Q)/cc-pVTZ level of theory.

(2) $O_2^+(X\ ^2\Pi_g) + N(^4S)$ Charge-Transfer Products. As shown in Figure 4, the reaction on the Q_2 potential surface goes through a very high barrier, **Q_2_TS1**, that is over 1 eV higher in energy than either the $N(^2D) + O_2^+(X\ ^2\Pi_g)$ product asymptote or the reactants. Thus, crossing of the $N(^2D) + O_2^+(X\ ^2\Pi_g)$ singlet and triplet PESs associated with the $N(^2D) + O_2^+(X\ ^2\Pi_g)$ asymptote at relatively large reactant distance to Q_2 is possible. Many crossing points should exist between the $N(^2D) + O_2^+(X\ ^2\Pi_g)$ asymptote (formed above by charge transfer from the $N^+(^3P) + O_2(^3\Sigma_g)$ reactants) and the Q_2 state, which will give the $O_2^+(X\ ^2\Pi_g)$ product together with the ground-state $N(^4S)$. Since this is an intersystem crossing (singlet−quintet and triplet−quintet) process with weak spin−orbit interaction, one expects that this will be of minor importance as the source of the experimentally observed $O_2^+(X\ ^2\Pi_g)$ product.

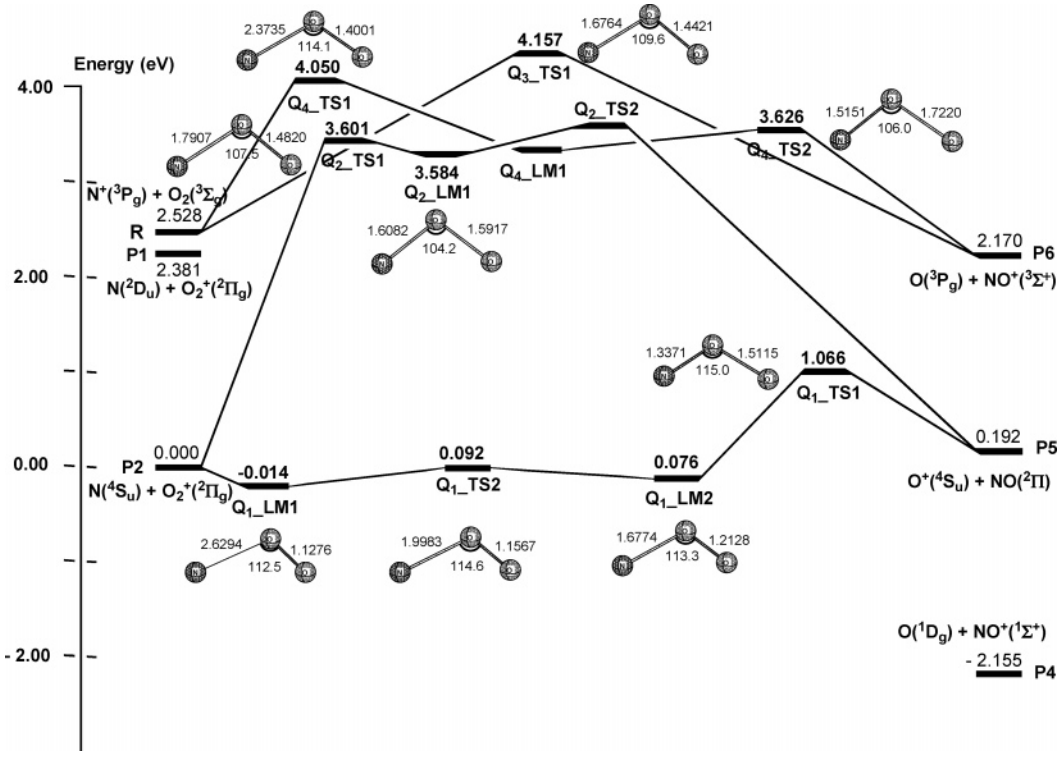

Figure 4. MRCISD(Q)/aug-cc-pVQZ potential energy profiles of the quintet states (Q_1-Q_4) in the $N^+ + O_2$ reaction. The numbers on the structures are bond length (Å) and bond angle (deg). The geometries were optimized at the state-specific CASPT2(15e,12o)/cc-pVTZ level of theory, and the energetics was calculated at the state-specific MRCISD(Q)(15e,12o)/aug-cc-pVQZ level.

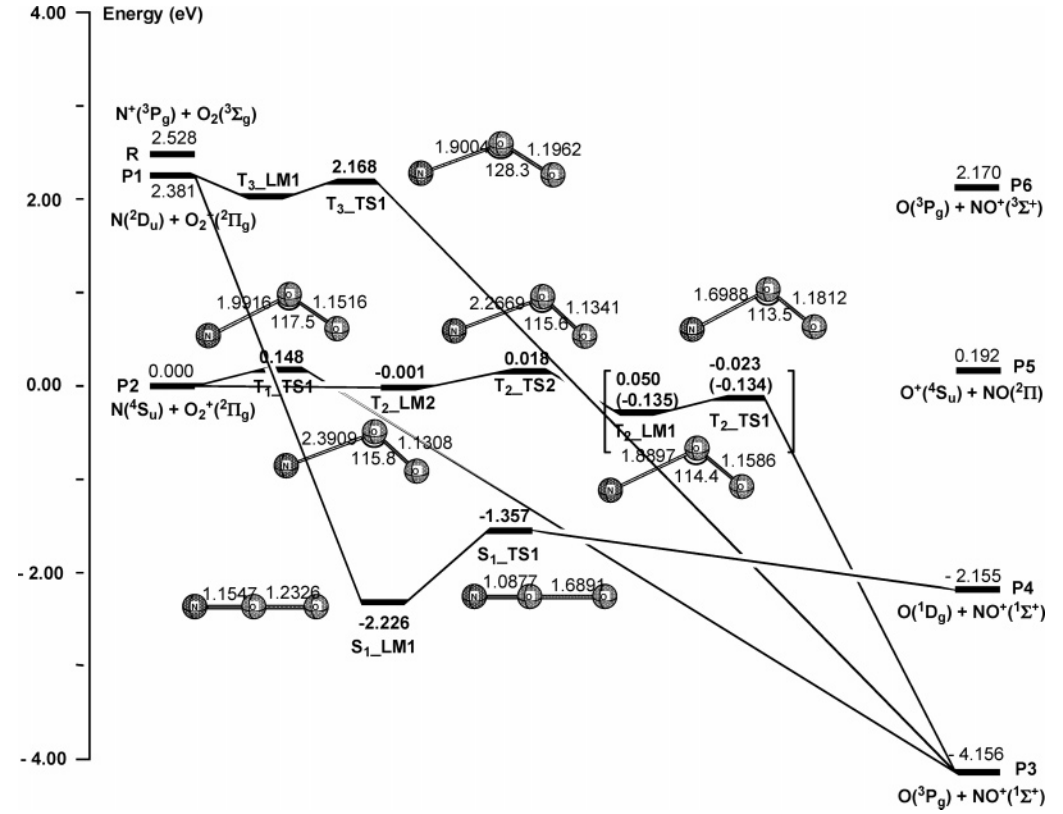

Figure 5. MRCISD(Q)/aug-cc-pVQZ potential energy profiles of the T_1, T_2, T_3, and lowest singlet state involved in the $N^+ + O_2$ reaction. See Figure 4 for details. Numbers in the parentheses are the values calculated at the level of geometry optimization.

(3) $NO^+(X\ ^1\Sigma^+)$ Products. As shown in the adiabatic correlation diagram in Figure 2, the T_1-T_3 and S_1-S_5 surfaces will contribute to the formation of $NO^+(X\ ^1\Sigma)$. The $T_1(1^3A')$ and $T_2(1^3A'')$ pathways originate from the $N(^4S) + O_2^+(X\ ^2\Pi_g)$ spin-forbidden channel and are therefore expected to be of minor importance. The $T_3(2^3A'')$ and S_1-S_5 pathways originate from the favored $N(^2D) + O_2^+(X\ ^2\Pi_g)$ charge transfer channel and produce $NO^+(X^1\Sigma)$ with $O(^3P)$ and $O(^1D)$, respectively. The adiabatic potential energy profiles for these processes are shown in Figure 5. The lowest energy singlet $S_1(1^1A')$ pathway has

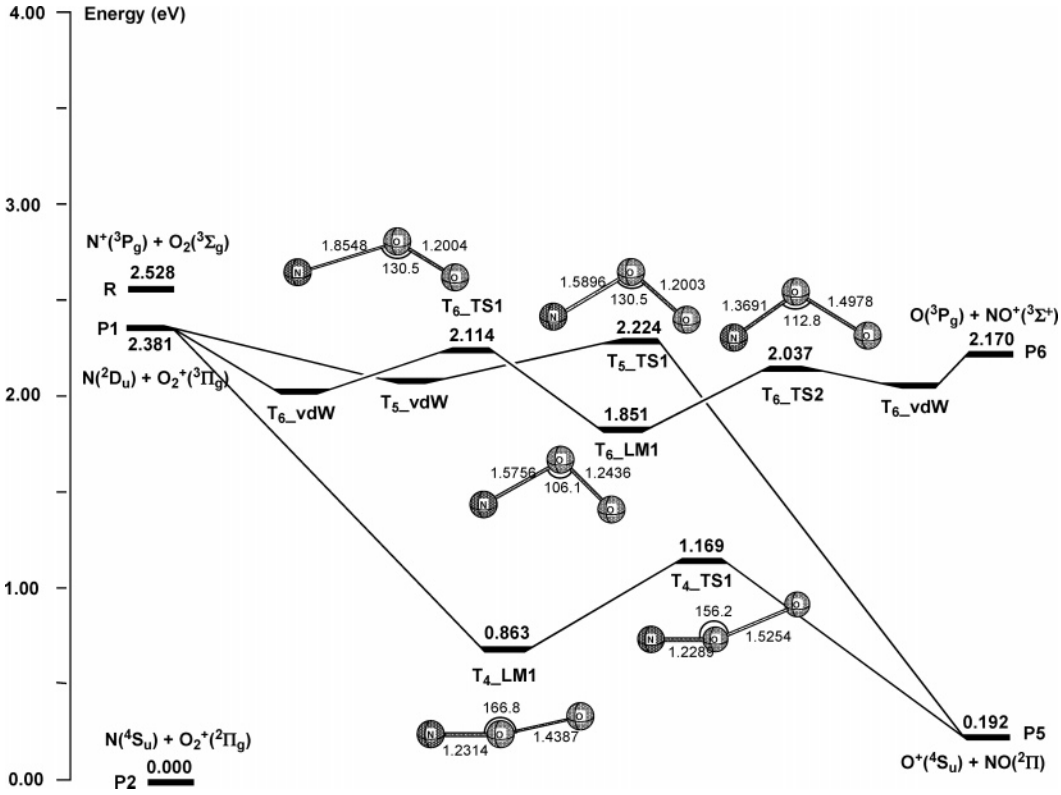

Figure 6. MRCISD(Q)/aug-cc-pVQZ potential energy profiles of the T_4, T_5, and T_6 states in the $N^+ + O_2$ reaction. See Figure 4 for details.

been examined in our previous study of $N_3^+ + O_2$ (see Figure 4 of ref 34). In this pathway, the formation of an NOO^+ intermediate (**S_1_LM1**) from the $N(^2D) + O_2^+(X\ ^2\Pi_g)$ charge transfer channel is barrierless and extremely exothermic, having an overall exothermicity of about 4.75 eV from the $N^+(^3P) + O_2(X\ ^3\Sigma_g)$ reactants. The dissociation of **S_1_LM1** to give $O(^1D) + NO^+(X\ ^1\Sigma^+)$ only needs to cross over a barrier at **S_1_TS1** of 0.87 eV, and this S_1 pathway is expected to be a major channel for the production of $NO^+(X\ ^1\Sigma^+)$. It was also found in the previous study that two minima of seams-of-crossing with a strong spin−orbit interaction exist between this singlet state and the triplet state located about 0.1 eV below the dissociation transition state **S_1_TS1**.[34] This nonadiabatic transition can produce the $O(^3P_g) + NO^+(X\ ^1\Sigma^+)$ product, although this pathway is of minor importance. Other than the lowest singlet state, no stationary structures were found on the second and third singlet states and no additional calculations were performed beyond these three states due to the computational costs.

The reaction on the T_3 triplet surface from the $N(^2D) + O_2^+(X\ ^2\Pi_g)$ charge transfer channel will directly proceed to the $O(^3P) + NO^+(X\ ^1\Sigma^+)$ products through **T_3_TS1** that is about 0.2 eV below the $N(^2D) + O_2^+(X\ ^2\Pi_g)$ asymptotic limit, indicating that a van der Waals complex must exist, labeled **T_3_LM1** in Figure 5. A search for this minimum was not successful; however, finding this species is relatively unimportant for understanding the reaction mechanism. Since the barrier is below the reactant energy, one expects that this reaction channel is also important for producing $NO^+(X\ ^1\Sigma^+)$. In the experiments, the $NO^+(X\ ^1\Sigma^+)$ product can be detected, but the electronic state of the associated O atom fragment cannot be inferred. To determine the branching ratio for the different O atom states, detailed dynamics calculations would have to be carried out. Nevertheless, the above discussions based in Figure 5 suggest that starting from the $N(^2D) + O_2^+(X\ ^2\Pi_g)$ charge transfer channel, the S_1 pathway to give $O(^1D) + NO^+(X\ ^1\Sigma^+)$ products without a significant barrier and with an extremely large exothermicity is likely to be the most important reactive channel. The T_3 pathway to give $O(^3P) + NO^+(X\ ^1\Sigma^+)$ products with a modest barrier also contributes to the formation of NO^+.

(4) $NO^+(a\ ^3\Sigma^+)$ Products. Figure 2 shows that both the Q_3 and Q_4 states of the reactants, $N^+(^3P) + O_2(X\ ^3\Sigma_g)$, correlate adiabatically to the $O(^3P) + NO^+(a\ ^3\Sigma^+)$ product. However, as shown in Figure 4, the reactions on both of these states require at least 1.5 eV of activation energy to access either **Q_4_TS1** or **Q_3_TS1**. Therefore, any formation of NO^+(a) products must come from the singlet (S_6−S_8) and triplet (T_6−T_8) states, starting from the charge transfer channel $N(^2D) + O_2^+(X\ ^2\Pi)$. Due to the computational cost, only the relatively lower energy excited-state T_6 ($3^3A'$) was investigated, and its potential energy profile is shown in Figure 6. Reaction on this pathway will first pass through **T_6_TS1** to form a NOO^+ intermediate, **T_6_LM1**. The energy of the TS is lower than that of the dissociation limit, which suggests the existence of a van der Waals complex; although we did not determine this structure, it does not preclude understanding of the reaction mechanism. The intermediate **T_6_LM1** is quite stable, about 0.5 eV lower in energy than the charge transfer asymptote $N(^2D) + O_2^+(X\ ^2\Pi)$, but it dissociates to the $NO^+(a\ ^3\Sigma^+)$ product with a low activation energy of only around 0.2 eV at **T_6_TS2**. Through this mechanism, reaction from the $N(^2D) + O_2^+(X\ ^2\Pi_g)$ channel will give rise to the $NO^+(a\ ^3\Sigma^+)$ product. Although no calculation was performed on the remaining higher excited states responsible for the NO^+(a) product, it is expected that the energy requirement for these states is higher than that of T_6. In addition, the large exothermic reactions on the lower excited states (e.g. S_1 and T_3) will make this channel energetically less favorable. Therefore, only a limited amount of $NO^+(a\ ^3\Sigma^+)$ will be formed as confirmed in the experiments.

(5) $O^+(^4S)$ Products. The production of $O^+(^4S)$ can take place either via the triplet ($T_4(2^3A'$) and $T_5(3^3A'')$) or the quintet ($Q_1(1^5A'$) and $Q_2(1^5A'')$) PESs associated with the $N(^2D) + O_2^+(X\ ^2\Pi_g)$ and $N(^4S) + O_2^+(X\ ^2\Pi_g)$ asymptotes, respectively, as

shown in Figure 2. The potential energy profiles for the triplet ($T_4(2^3A')$ and $T_5(3^3A'')$) pathways are shown in Figure 6. The formation of $O^+(^4S)$ on the T_5 state was found to go over a low-energy TS, **T_5_TS1**, whose energy is about 0.16 eV lower than that of the dissociation limit of $N(^2D) + O_2^+(X\ ^2\Pi_g)$, indicating the existence of a van der Waals complex before this TS. On the T_4 state, a stable NOO^+ type structure, **T_4_LM1**, was identified at 1.52 eV below $N(^2D) + O_2^+(X\ ^2\Pi_g)$ asymptote, which can be reached downhill without a transition state. The dissociation of **T_4_LM1** will directly lead to the $O^+(^4S)$ species via a low barrier, **T_4_TS1**, which is located at 0.31 eV above **T_4_LM1**. Since the channels producing $NO^+(X\ ^1\Sigma^+)$ have more favorable energetics, these two channels will be less important contributors to the overall reaction. However, the lower energy requirement will obviously favor $O^+(^4S)$ over $NO^+(a\ ^3\Sigma^+)$ product, which is consistent with the experimental results. More quantitative branching ratios can be justified only from a detailed dynamics study.

The potential energy profiles of the $Q_1(1^5A')$ and $Q_2(1^5A'')$ states from the $N(^4S) + O_2^+(X\ ^2\Pi_g)$ product asymptote to the O^+ product are shown in Figure 4. Reaction on the Q_1 pathway has a barrier of 1.1 eV above the $N(^4S) + O_2^+(X\ ^2\Pi_g)$ asymptote, which is well below the $N^+(^3P) + O_2(X\ ^3\Sigma)$ reactants. This process may be fast; however, it will be a minor contributor to the products observed, again due to the limited amount of $N(^4S) + O_2^+(X\ ^2\Pi_g)$ formed. The reaction on the Q_2 state has a high barrier at **Q_2_TS1**, which is about 1.1 eV higher than the $N^+(^3P) + O_2(X\ ^3\Sigma)$ reactants and is, thus, unimportant.

The calculations above show remarkable complexity for this three-atom system. It appears that the charge transfer to the $N(^2D) + O_2^+(X\ ^2\Pi_g)$ channel takes place predominantly at a very early stage, which gives rise to the $N(^2D) + O_2^+(X\ ^2\Pi_g)$ product and at the same time serves as the starting point for all the reactive channels producing $NO^+(^1\Sigma^+)$ (major product, via S_1 and T_3 pathways), $O^+(^4S)$ (minor product, via T_4 pathway), and $NO^+(a\ ^3\Sigma^+)$ (minor product, via T_6 pathway), although other channels may make additional minor contributions. These pathways qualitatively explain why the excited $NO^+(a\ ^3\Sigma^+)$ is produced with such a small branching ratio. Production of excited N atoms is important as explained below.

(6) Atmospheric Implications. The NO concentration in the thermosphere is controlled in part by ionic processes which produce $N(^2D)$ and $N(^4S)$.[35] Most of the $N(^2D)$ produced reacts with O_2 to produce NO,

$$N(^2D) + O_2 \rightarrow NO + O \qquad (2)$$

In contrast, $N(^4S)$ leads to NO destruction because the reaction of $N(^4S)$ with O_2 is slow,

$$N(^4S) + O_2 \rightarrow NO + O \qquad (3)$$

Instead, most of the $N(^4S)$ reacts with NO,

$$N(^4S) + NO \rightarrow N_2 + O \qquad (4)$$

thereby destroying NO. Other minor processes also occur. Thus, the balance of NO in this region is strongly influenced by the ratio of $N(^4S)$ to $N(^2D)$, in part through reaction 1. Other important ionic sources of N atoms include the recombination of NO^+ and N_2^+ and the reaction of N_2^+ with O atoms.

Conclusions

The distribution into the first two electronic states of NO^+ produced in the reaction of N^+ with O_2 has been probed at 298 and 500 K. Only ca. 1% of the NO^+ product ions are formed in the $NO^+(a\ ^3\Sigma^+)$ excited state at both temperatures. For the overall reaction mechanism of N^+ with O_2, the present ab initio calculations showed that charge transfer proceeds through a large number of electronic excited states involving several crossings on the potential energy surface to reach the product ion surfaces. A pathway leading to the $NO^+(a\ ^3\Sigma^+)$ product has been identified and has been found to be less favorable than the major channels leading to the $NO^+(X\ ^1\Sigma^+)$ product. Interestingly, a large fraction of the neutral N atoms associated with $O_2^+(X\ ^2\Pi_g)$ should be $N(^2D)$. These results provide new insight into the complex chemistry of an important atmospheric ion−molecule reaction process.

Acknowledgment. We acknowledge Jürgen Troe's tremendous influence on chemical kinetics and his inspiration. A.A.V., in particular, thanks Jürgen for not only a close collaboration over the last years but also a close friendship. A.J.M. and A.A.V. thank John Williamson and Paul Mundis for technical support of the experiments. The experimental work is supported by the Air Force Office of Scientific Research under Task No. 2303EP4. A.J.M. is supported through Boston College Contract No. FA8718-04-C-0006. The theoretical work was in part supported by the Air Force Office of Scientific Research (Grant FA9550-04-1-0080). Computer resources were provided in part by the Air Force Office of Scientific Research DURIP Grant FA9550-04-1-0321 as well as by the Cherry Emerson Center for Scientific Computation at Emory University and by a grant from AFOSR under the DoD High Performance Computing Program.

References and Notes

(1) *Handbook of Geophysics and the Space Environment*; Jursa, A. S., Ed.; National Technical Information Service: Springfield VA, 1985.
(2) Ferguson, E. E.; Fehsenfeld, F. C.; Albritton, D. L. In *Gas-Phase Ion Chemistry*; Bowers, M. T., Ed.; Academic: San Diego, CA, 1979; Vol. 1, pp 45−82.
(3) Banks, P. M.; Kockarts, G. *Aeronomy*; Academic: New York, 1973.
(4) Lindinger, W.; Fehsenfeld, F. C.; Schmeltekopf, A. L.; Ferguson, E. E. *J. Geophys. Res.* **1974**, *79*, 4753.
(5) Tully, J. C.; Herman, Z.; Wolfgang, R. *J. Chem. Phys.* **1971**, *54*, 1730.
(6) Dotan, I.; Hierl, P. M.; Morris, R. A.; Viggiano, A. A. *Int. J. Mass Spectrom. Ion Phys.* **1997**, *167/168*, 223−230.
(7) Smith, M. A.; Bierbaum, V. M.; Leone, S. R. *Chem. Phys. Lett.* **1983**, *94*, 398.
(8) Dreyer, J. W.; Perner, D. *Chem. Phys. Lett.* **1971**, *12*, 299.
(9) Albritton, D. L.; Viggiano, A. A.; Dotan, I.; Fehsenfeld, F. C. *J. Chem. Phys.* **1979**, *71*, 3295.
(10) Howorka, F.; Dotan, I.; Fehsenfeld, F. C.; Albritton, D. L. *J. Chem. Phys.* **1980**, *73*, 758.
(11) Langford, A. O.; Bierbaum, V. M.; Leone, S. R. *Space Sci.* **1985**, *33*, 1225−1228.
(12) Langford, A. O.; Bierbaum, V. M.; Leone, S. R. *J. Chem. Phys.* **1986**, *84*, 2158.
(13) McFarland, M.; Albritton, D. L.; Fehsenfeld, F. C.; Ferguson, E. E.; Schmeltekopf, A. L. *J. Chem. Phys.* **1973**, *59*, 6620−6628.
(14) Johnsen, R.; Brown, H. L.; Biondi, M. A. *J. Chem. Phys.* **1970**, *52*, 5080.
(15) Smith, D.; Adams, N. G.; Miller, T. M. *J. Chem. Phys.* **1978**, *69*, 308.
(16) Farragher, A. L. *Trans. Faraday Soc.* **1970**, *66*, 1411.
(17) Guettler, R. A.; Jones, G. C.; Posey, L. A.; Kirchner, N. J.; Keller, B. A.; Zare, R. N. *J. Chem. Phys.* **1994**, *101*, 3763.
(18) O'Keefe, A.; Mauclaire, G.; Parent, D.; Bowers, M. T. *J. Chem. Phys.* **1986**, *84*, 215.
(19) Viggiano, A. A.; Knighton, W. B.; Williams, S.; Arnold, S. T.; Midey, A. J.; Dotan, I. *Int. J. Mass Spectrom.* **2003**, *223−224*, 397−402.
(20) Dotan, I.; Fehsenfeld, F. C.; Albritton, D. L. *J. Chem. Phys.* **1979**, *71*, 3280.
(21) Dotan, I.; Fehsenfeld, F. C.; Albritton, D. L. *J. Chem. Phys.* **1979**, *71*, 3289.
(22) Glosik, J.; Rakshit, A. B.; Twiddy, N. D.; Adams, N. G.; Smith, D. *J. Phys. B: Atom. Mol. Phys.* **1978**, *11*, 3365.

(23) Viggiano, A. A.; Morris, R. A.; Dale, F.; Paulson, J. F.; Giles, K.; Smith, D.; Su, T. *J. Chem. Phys.* **1990**, *93*, 1149−1157.
(24) Midey, A. J.; Viggiano, A. A. *J. Chem. Phys.* **1998**, *109*, 5257.
(25) Celani, P.; Werner, H.-J. *J. Chem. Phys.* **2000**, *112*, 5546.
(26) Kendall, R. A.; Dunning, T. H., Jr.; Harrison, R. J. *J. Chem. Phys.* **1992**, *96*, 6796.
(27) Knowles, P. J.; Werner, H.-J. *Chem. Phys. Lett.* **1988**, *145*, 514.
(28) Langhoff, S. R.; Davidson, E. R. *Int. J. Quantum Chem.* **1974**, *8*, 61.
(29) Davidson, W. R. *J. Comput. Chem.* **1975**, *17*, 87.
(30) Ikezoe, Y.; Matsuoka, S.; Takebe, M.; Viggiano, A. A. *Gas-Phase Ion−Molecule Reaction Rate Constants Through 1986*; Maruzen Co., Ltd.: Tokyo, 1987.
(31) Hierl, P. M.; Dotan, I.; Seeley, J. V.; Van Doren, J. M.; Morris, R. A.; Viggiano, A. A. *J. Chem. Phys.* **1997**, *106*, 3540−3544.
(32) Fukuzawa, K.; Matsushita, T.; Morokuma, K. *J. Chem. Phys.* **2004**, *121*, 3117−3129.
(33) Fukuzawa, K.; Matsushita, T.; Morokuma, K.; Levandier, D. J.; Chiu, Y.-H.; Dressler, R. A.; Murad, E.; Midey, A. Viggiano, A. A. *J. Chem. Phys.* **2001**, *115*, 3184.
(34) Popovic, S.; Midey, A. J.; Williams, S.; Fernandez, A.; Viggiano, A. A.; Zhang, P.; Morokuma, K. *J. Chem. Phys.* **2004**, *121*, 9481−9488.
(35) Brasseur, G.; Solomon, S. *Aeronomy of the Middle Atmosphere*, 2nd ed.; D. Reidel: Boston, MA, 1986.